Insights in the Phenomena Involded in Deactivation of Industrial Hydrocracking Catalysts Through an Accelerated Deactivation Protocol

July Vivas-Báez, Alberto Servia, Gerhard Pirngruber, Anne-Claire Dubreuil, David J Pérez-Martínez

INSIGHTS IN THE PHENOMENA INVOLVED IN DEACTIVATION OF INDUSTRIAL HYDROCRACKING CATALYSTS THROUGH AN ACCELERATED DEACTIVATION PROTOCOL

July C.VIVAS-BÁEZ[ab], Alberto SERVIA[a], Gerhard PIRNGRUBER[a], Anne-Claire DUBREUIL[a], David J. PÉREZ-MARTÍNEZ[b]

a IFP Energies nouvelles, Rond-point de l'échangeur de Solaize, France, 69360.
b Centro de innovación y tecnología ICP, ECOPETROL S.A., Km 7 vía Piedecuesta, Piedecuesta, Colombia, 681011.
Corresponding Author: Gerhard PIRNGRUBER (gerhard.pirngruber@ifpen.fr)

ABSTRACT

A representative accelerated experimental deactivation procedure was developed to understand the activity loss of bifunctional vacuum gasoil (VGO) hydrocracking catalysts over time. Experiments were performed in an up-flow fixed-bed pilot unit with a typical vacuum gas oil feedstock. The deactivation was measured by tracking the decrease of VGO conversion (370°C$^+$) with time on stream. The catalyst consisted of nickel-molybdenum sulfide particles dispersed on a carrier containing USY zeolite. The impact of temperature, liquid hourly space velocity (LHSV), hydrogen to hydrocarbon (H_2/HC) ratio and organic nitrogen (N_{org}) on the catalyst deactivation rate was firstly studied. The variables with the most significant impact on conversion loss were temperature and space velocity. Temperature directly influences the production rate of coke precursors, whereas space velocity affects the local concentration of feed contaminants along the reactor. Based on these results, the following operating conditions were selected to establish the final accelerated deactivation experimental protocol: T=418°C, LHSV=3 h^{-1}, H_2/HC=1500NL/L, P=14 MPa, organic nitrogen content (N_{org})=150 ppm weight, total nitrogen content=2500 ppm weight and a total time on stream of 30 days. Spent samples from this procedure presented similar properties to some industrial catalysts submitted to cycle lengths between 12 and 18 months. Both types of samples yield similar values of surface area and pore volume loss as well as a similar amount and nature of coke deposits. These results led to the qualitative validation of the protocol representativeness. This experimental procedure was then used to

get more insight into the deactivation phenomenon. It was found that the organic nitrogen content of the feedstock is crucial, as it determines the ratio between available metal and acid sites. This ratio determines the reactions that take place and, therefore, the type of coke produced.

Keywords: deactivation, hydrocracking, coking, vacuum gasoil.

INTRODUCTION

Hydrocracking is one of the most flexible refining processes for converting heavy high-boiling feedstock molecules into smaller lower-boiling products. Hydrocracking processes are operated at high pressure, 8.5-20 MPa, and moderate temperature, 350-450°C, to promote hydrocracking reactions. A large excess of hydrogen, 500-1700 NL/L hydrogen to oil ratio (H_2/HC), is fed to the reactor to improve liquid yield and limit catalyst deactivation. Low values of LHSV, 0.5-2.5 h^{-1}, are required depending on feed nature and complexity [1]. The feedstocks used in hydrocracking processes contain sulfur, nitrogen and, in the case of residue feedstocks, metals such as nickel and vanadium [1]. Due to the deleterious effect of these compounds on hydrocracking catalysts, the hydrocracking process is carried out in two consecutive stages: (i) in the first stage, the feedstock is hydrotreated and partially hydrogenated on a hydrotreating catalyst. The main chemical reactions for hydrotreating and hydrogenating the feedstock are hydrodesulfurization (HDS), hydrodenitrogenation (HDN), hydrodeoxygenation (HDO), olefin hydrogenation and partial aromatics hydrogenation. (ii) In the second stage, the hydrotreated feed is hydrocracked on a hydrocracking catalyst [2]. This work focuses on the deactivation phenomena related to the catalyst of the second stage of a typical hydrocracking process.

Hydrocracking catalyst deactivation under typical industrial operating conditions occurs slowly, depending on feed and operation severity. Cycle lengths can vary between a few months and up to one or two years [9–11]. One cycle involves the processing of

approximately 5000 tons of feed per ton of catalyst [12]. The loss of activity determines the length of an operation cycle and, consequently, profitability [11]. Catalyst deactivation is inevitable, but it can be slowed down [9,13,14]. Understanding the deactivation phenomena is fundamental for the design of more stable catalysts.

Based on the literature on catalyst deactivation related to several refinery applications such as hydrotreating, heavy oil hydroprocessing and catalytic reforming, two main approaches for the study of this complex phenomena can be distinguished. The first one is based on the characterization of industrial-spent catalyst samples to link coke or metal deposition to catalyst deactivation. This approach has, for instance, been applied to the hydroprocessing of diesel, vacuum gasoil (VGO) and vacuum residue [6,15]. Understanding deactivation phenomena through this specific approach is limited as feed and operating conditions continuously change during industrial operation. This approach does not allow to link these parameters to the extent of deactivation, as the spent catalyst is characterized only once at the end of the industrial cycle. Another approach could consist of performing experiments at equivalent industrial conditions in the laboratory [16]. This approach can be expensive and time-consuming, as industrial cycle lengths can be up to two years. Hence, the development of accelerated deactivation procedures, which is the second approach for studying deactivation, appears as an instrument capable of providing relevant information on the deactivation phenomena in a reduced time [16,17]. Accelerated deactivation consists of submitting the catalyst to specific reaction conditions that strongly promote deactivation [18]. On the one hand, the accelerated methodology allows performing a kinetic evaluation [17,18] based on the activity loss between the beginning and the end of the operation. And on the other hand, this methodology includes the detailed characterization of the deactivated catalysts, which is more valuable for assessing the changes in catalyst properties [3].

The specific deactivation mechanisms of vacuum gasoil (VGO) hydrocracking catalysts are now addressed. The industrial catalysts are bifunctional, i.e., composed of metal sulfide nanoparticles (hydrogenation/dehydrogenation function) deposited on an acidic support

(isomerization and cracking function). This catalyst is continuously deactivated in the presence of hydrocarbon feedstocks under typical hydrocracking process operating conditions. The primary sources of deactivation are coke formation and quasi-irreversible poisoning by heavy nitrogen molecules [3,4]. These phenomena depend on feedstock, operating conditions and catalyst properties such as catalyst acidity, nature of the sulfide phase and support porosity [5]. The coke formation is related to polymerization precursors like polynuclear aromatics and cyclic molecules containing heteroatoms [3,6]. Both metal sulfide nanoparticles and acid sites are deactivated by coke deposition[3]. Other deactivation mechanisms can also occur as sintering and de-promotion of the sulfide nanoparticles and strong adsorption (almost irreversible) of nitrogen compounds [1,3,5,7] (that can act as temporary poisons[4]) on the acid sites.

Nitrogen compounds can act as inhibitors or poisons, depending on their structure and properties. Poisoning refers to the strong chemisorption of reactants, products, or impurities on active sites that would normally be available for catalysis in the absence of these poison compounds. Inhibition results from the reversible adsorption of a given nitrogen compound. The main difference between both mechanisms is that, in the case of inhibition, the catalyst regains its original activity after inhibitor removal from the feedstock. Thus, an inhibitor is not a real poison since it only temporarily competes for active sites. An actual poison is not desorbed; its bonding to the active site is so strong that its desorption rate is negligible under reaction conditions [3,6]. The poison gradually neutralizes the catalytic sites along the catalyst bed. In vacuum gasoil hydrocracking, two types of nitrogen molecules can be distinguished: ammonia produced by the hydrodenitrogenation (HDN) reactions and residual organic nitrogen compounds. The residual organic nitrogen compounds in hydrocracking feedstocks can be divided into two families: low-basicity or "neutral" nitrogen compounds, such as pyrrole homologues, and basic nitrogen compounds such as pyridine homologues and amines [1,4]. The lightest basic or neutral nitrogen derivatives are readily decomposed into ammonia, which acts as an inhibitor of the cracking reaction, whereas the more basic

compounds are cataloged as poisons as they are strongly adsorbed on the acid sites of the catalyst [8].

Regarding coking, a major part of the studies in literature, for instance, the works of Muegge [19,20], Zeuthen [21], and Guichard [18], was carried out by using model molecules. The selected molecules were not fully representative of the real components of the industrial feed, and the deactivation mechanisms were different from those in real feeds. In the case of hydrocracking catalysts, Dujardin [7] only identified "soft coke" (high H/C ratio) in the spent catalysts as the deactivation experiments were performed with n-heptane.

Concerning works with real feedstocks, Tanaka et al. [14] conducted tests with VGO under high severity conditions to evaluate coke deposition effects on the hydrotreating process. They concluded that a higher temperature and a heavier feed resulted in a serious carbonaceous deposition, which did not fully represent industrial deactivation. Ahmed et al. [22] studied the loss of catalyst activity during the hydrocracking of a vacuum residue under accelerated deactivation conditions. A high reaction temperature was imposed for catalyst accelerated aging, resulting in large amounts of carbonaceous deposits with high aromaticity. This result was attributed to a decrease in the hydrogenation activity of the catalyst due to coke and metal deposition on sulfide nanoparticles. Figoli [23] studied the deactivation of a Pt-catalyst during naphtha reforming through a protocol that consisted of the three following stages: 10 h under typical reforming conditions to obtain a RON of 95, then 10 h at a lower hydrogen pressure to obtain rapid coke deposition and finally 10 h where the temperature was increased until the RON of the first stage was reached. With this protocol, a coke of similar nature as the one produced in a commercial plant was obtained.

To the best of our knowledge, a representative experimental procedure for studying this phenomenon is missing in that specific case. The first objective of this work was to develop an accelerated deactivation protocol to study the deactivation phenomena under representative conditions of the industrial operation. Aged catalysts from this procedure were

characterized for the determination of their porosity, the quantity and nature of coke deposits and the residual activity of their two catalytic functions, acid and metal. The results were compared to the characterization results of industrial spent catalysts for the qualitative validation of the accelerated deactivation procedure. The second and final aim of this study was to get insights into the VGO hydrocracking catalysts deactivation phenomenon itself through this specific experimental procedure.

EXPERIMENTAL SECTION

Pilot unit description

The experiments were carried out in a fixed bed pilot unit with a co-current gas-liquid mixture flowing upwards to ensure complete catalyst wetting. The flow diagram of the unit is shown in **Figure 1**. The unit consists of a feed, a reaction and separation sections with an online chromatograph for determining the outlet gas stream composition. The feed section consists of a storage tank filled with the process feed and pressurized with nitrogen. The content of this storage tank was transferred to a smaller intermediate tank employing a pump. The feed flow rate was controlled based on the decrease in weight measured by a balance on which the intermediate tank was supported. The feedstock was injected into the reactor using a positive displacement pump. A mass flowmeter controlled hydrogen flow. Feed and hydrogen were mixed upstream of the reaction section and flowed concurrently in an upflow configuration. The pilot unit has two tubular reactors in series (R1 and R2 in the figure below). Each reactor was placed within a furnace presenting three independent heating zones. Each zone was equipped with internal and external thermocouples to ensure isothermal conditions (the thermal profile was measured at the beginning of the test in which the screening of the operating variables was performed – see section 0). The two reactors were used for the hydrocracking process; or in other words, the feed used in this work was hydrotreated ex-situ.

Additionally, a sampling system allowing the liquid phase effluent from the first reactor to be collected and analyzed was placed between the two reactors. The samples taken at this point contained some dissolved gases, including hydrogen sulfide and ammonia. Therefore, these samples were washed with water to eliminate these gases, allowing their properties to be accurately measured. To calculate the net conversion obtained in the first reactor, the gas formation was estimated from the correlation established between both gas and liquid yields. The effluent of the second reactor was then sent to the separation section. This section comprises a high-pressure flash separator for gas/liquid separation. The gas-phase was continuously recovered at the top of the separator under pressure control. The gas effluent was transferred to a gas flowmeter, and a sample was taken for online gas chromatographic analysis. The liquid product was continuously recovered at the bottom of the separator, under level control, and sent to a low-pressure hydrogen stripper. The stripper conditions were adjusted for removing the residual hydrogen sulfide and ammonia dissolved in the products. The stripped product was finally sent to a storage recipient equipped with a balance to quantify the amount of product obtained. Liquid products were characterized by density, refraction index, nitrogen and sulfur content and simulated distillation.

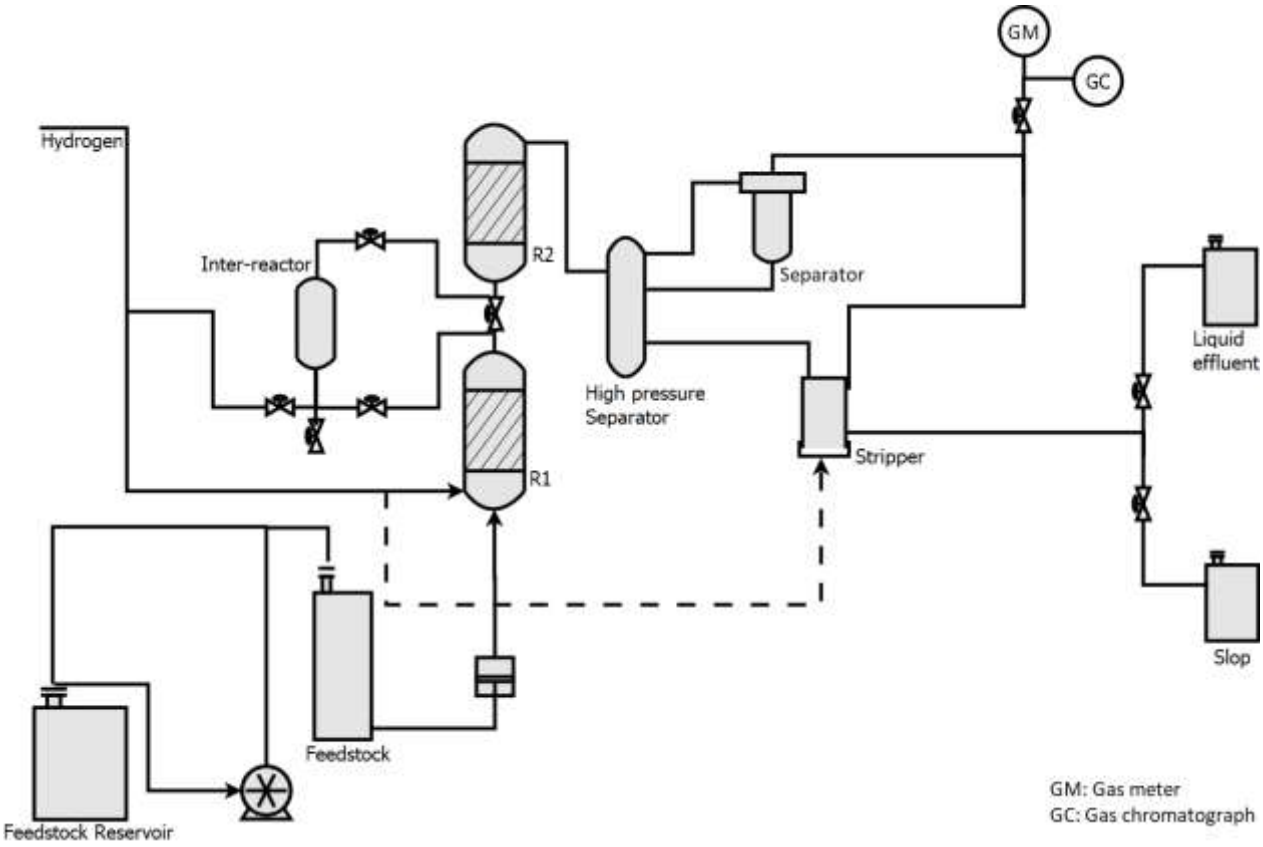

Figure 1. Pilot unit flow diagram.

Procedure for the pilot plant experiments

Each experiment started with the in situ catalyst sulfidation with an atmospheric gasoil (d15:0.8491 g/cm^3) spiked with 2% wt %/feed. of dimethyl disulfide (DMDS) and 2% wt %/feed. of aniline, at 350°C. After catalyst sulfidation, the operating conditions were imposed (temperature ranging from 374 to 418°C and LHSV between 1.5 and 3 h^{-1} depending on the specific experiment). A mass balance and relevant gas and liquid analysis were carried out after catalyst stabilization for accurate catalyst performance measurement. Unit stabilization was tracked through the monitoring of the liquid effluent density. The performance was considered stable when the density variation was lower than 0.0010 g/cm^3 for 24 consecutive hours. Once this condition is reached, the catalyst performance evaluation was launched and the process continued at the same operating conditions until the desired evaluation time is completed. At the end of the experiment, the temperature was decreased to 350°C, and the feed switched to the atmospheric gasoil to wash both the unit and the catalyst at constant

pressure and hydrogen flow. Afterward, the feed flow was stopped and the catalyst was stripped and dried at a reduced pressure of 2 MPa in the presence of hydrogen. At the end of the experiment, the temperature was reduced to ambient conditions. The unit was purged with nitrogen to ensure inert conditions and then depressurized. The catalyst was finally unloaded by following the specific procedure described in section 2.3.3.

Pilot unit validation

Before developing the accelerated deactivation protocol, a reference test was executed to ensure that experiments are carried out in the so-called kinetic-regime. This test was performed with the fresh catalyst described in section 2.2.2 and a hydrotreated VGO (**Table 1**) similar to the one used in the rest of the experimental plan but with lower nitrogen content. The criterion to be fulfilled for pilot plant validation is the performance similarity compared to a more representative unit of 200 cm^3, which is four times bigger than the fixed-bed used in this work. The operating conditions for this test are presented in Table 2. The global operation was validated as mass balances were respected with deviations lower than 2% weight. Both units present similar kinetic performances and a deviation between apparent activation energies lower than 2%. Therefore the performance of the pilot unit selected for this work can be considered as representative of a bigger unit used for scale-up purposes. The catalyst samples of this validation test were used as references (without deactivation) to compare samples from the deactivation experiment.

Table 1. Feedstock properties for the reference test.

Properties		VGO-HDT1
Density @ 15°C	g/cm^3	0.8787
Refraction Index @ 70° C		1.4627
Sulfur content	wt%	0.0054
Nitrogen Content	ppm	4.9
Yield of 370°C$^+$ fraction	wt%	79
Initial boiling point (IBP)	°C	110
Final boiling point (FBP)	°C	606

Table 2. Operating conditions of the reference test.

Point	P	T	H_2/HC	LHSV	Time*
	MPa	°C	NL/L	h^{-1}	Days
1	14	374	1000	1.5	11
2	14	380	1000	1.5	4
3	14	388	1000	1.5	5

*Including stabilization time

Materials

Feed Oil

The feedstock consisted of a hydrotreated vacuum gas oil (VGO-HDT2) containing around 150 ppm of organic nitrogen on a mass basis. This content was selected to accelerate catalyst deactivation. The main properties of this feed are shown in **Table 3**.

Table 3. Feedstock properties for the deactivation experiments.

Properties		VGO-HDT2
Density @ 15°C	g/cm^3	0.8984
Refraction Index @ 70° C		1.47505
Sulfur	wt%	0.068
Nitrogen	ppm	149
Aromatic carbon	%	10.3
Yield of 370°C+ fraction	wt%	92
Initial boiling point (IBP)	°C	179.8
Final boiling point (FBP)	°C	589.8

Dimethyl disulfide and aniline were added to the hydrotreated VGO to generate the hydrogen sulfide and ammonia partial pressures representative of the VGO mother feed. The mother feed contained a sulfur and a nitrogen content of 1.18 wt% and 0.22 wt%, respectively. The percentage of aromatic carbon was estimated through the n-d-M method according to the standard ASTM D3238.

Catalysts

The fresh catalyst consisted of nickel-molybdenum sulfide particles dispersed on a carrier containing USY zeolite.

The industrial spent catalyst samples were obtained from industrial units processing vacuum gas oils having densities ranging from 0.91 to 0.925 g/cm^3, sulfur mass percentage from 1 to 2% and nitrogen content from 1000 to 1400 ppm wt. They were unloaded by gravity at the end of the cycle, which lasted between 12 and 18 months.

Methods

Screening of operating variables

A screening of the operating variables was carried out to determine which key operating variables had the most impact on deactivation. The selected variables were temperature (T), space velocity (LHSV), hydrogen/hydrocarbon ratio (H_2/HC) and organic nitrogen (N_{org}). At the beginning of this procedure, the catalyst was submitted to the following reference case

(RC) conditions: 403°C, 14 MPa, H_2/HC = 1500 NL/L, LHSV = 2h^{-1}, total nitrogen and organic nitrogen content of 2200 ppm and 150 ppm in a mass basis, respectively. These conditions are within the operating window of a typical hydrocracking process. After catalyst stabilization, the temperature was changed and then kept constant for ten days, a period expected to be sufficient for evaluating the influence of each variable on deactivation. Afterward, the reference case conditions were restored and after catalyst stabilization, the loss in net conversion (**Equation 2**) caused by the variable under study was measured. The deactivating effect of each variable switch was evaluated by the difference between the conversions obtained at the reference conditions immediately before and after each operating variable switch. The procedure was repeated for all the variables mentioned above, as illustrated in **Figure 2** and **Table 4**.

Table 4. Operating conditions for the variables screening experiment.

Condition	P	T	H_2/HC	LHSV	N_{org}	N_{Total}
	MPa	°C	NL/L	h^{-1}	ppm	ppm
1 Reference case (RC)	14	403	1500	2	150	2200
2 Temperature	14	**410**	1500	2	150	2200
3 RC	14	403	1500	2	150	2200
4 H2/HC	14	403	**1000**	2	150	2200
5 RC	14	403	1500	2	150	2200
6 LHSV	14	403	1500	**3**	150	2200
7 RC	14	403	1500	2	150	2200
8 Norg	14	403	1500	2	**300***	2200
9 RC	14	403	1500	2	150	2200

* The feedstock was spiked with acridine, and carbazole, in a mass proportion of 1:3, respectively.

According to literature, the sequence selected for the variables evaluation was based on the expected impact of each operating parameter on deactivation rate. Thus, the variables expected to have a more significant impact on deactivation were tested at the beginning of the experiment.

Accelerated deactivation protocol

Based on the results obtained during the variables screening experiment, the following set of conditions was selected for the final accelerated deactivation protocol: T = 418°C, LHSV = 3 h^{-1}, H_2/HC = 1500NL/L, P = 14 MPa, with the feedstock spiked with aniline as described in Section 2.2.1 (N_{org} = 150 ppm wt., and N_{total} = 2500 ppm wt.) and a total time on stream of 30

days. The purpose of this protocol was to obtain a deactivated catalyst with properties similar to those related to industrial spent catalysts, with emphasis on the amount and nature of coke produced, as this is the primary mechanism of hydrocracking catalyst deactivation.

Catalyst loading and unloading procedures

Bed dilution is commonly used to minimize axial dispersion and gas-liquid mass transfer effects in pilot reactors [24]. In our case, bed dilution was performed by a direct mixture of the catalyst and inert particles of the same size as the catalyst. The dilution was carried out with silicon carbide particles of 1 mm diameter, and each reactor was loaded with 12.5 cm^3 of catalyst diluted with 37.5 cm^3 of silicon carbide. The mixture was divided into four small recipients, which were homogenized through manual shaking and then loaded into the reactor. The homogenization quality was previously checked in a glass reactor to ensure that the catalytic bed was uniform.

Catalyst samples taken at the end of each test run were carefully collected to separate the particles from the inlet and outlet of each catalytic bed. Different preliminary trials were carried out with a glass reactor in order to optimize this specific unloading protocol. Accurate catalyst unloading is very important since it allows to assess the evolution of catalyst properties depending on reactor location.

Catalyst characterization

Previous to catalyst characterization, samples were washed with toluene for 7 h in a soxhlet extractor at 250°C to remove the physically adsorbed hydrocarbons on the catalyst and dried under vacuum at 120°C for 12 h. The catalyst was characterized by the following analysis.

Nitrogen adsorption-desorption isotherms were measured in an ASAP 420 Micromeritics apparatus. The sample was submitted to a thermal pretreatment consisting of a temperature increase up to 100°C at 1°C/min, then a step of 30 min and after that, a new increase in temperature up to 500°C at 5°C/min with a step of 6 h under vacuum pressure (100 Pa). The

surface area was calculated from the BET equation, using data in the relative pressure range of p/p_0=0.05 to 0.3. The total pore volume was deduced from the N_2 adsorption at the endpoint of the isotherm. Micropore volume was determined from the t-plot method, with the Harkins-Jura formula, in the range of t from 0.35 to 0.50. The uncertainty of surface area and volume measurements is 5% and 2.5%, respectively. The pore size distribution was calculated from the desorption branch of the N_2 isotherm using the BJH model.

The carbon and nitrogen contents determination was carried out on a Thermoscientific FlashSmart equipment. Samples were pre-dried in situ at 290°C under helium flow for 15 minutes for water removal purposes to exclusively quantify the hydrogen directly bound to the coke. The uncertainties of measurement are 10% for carbon and 14% for nitrogen.

TGA of the deactivated catalysts was carried out on a thermobalance Mettler ToledoTGA-DSC1 coupled with mass spectroscopy (MS). The analysis has an uncertainty of 0.1% for the mass loss measurements. The sample was heated under a 25 cm^3/min air flow rate using a 5°C/min temperature ramp from 25 to 900°C. The effluents were qualitatively analyzed by an online mass spectrometer (Thermostar/Pfeiffer). The mass spectrometer signal recorded as a function of time allowed to qualified the nature of the emitted gas during sample decomposition. For estimating the H/C ratio, as the physisorbed water is eliminated at temperatures lower than 200°C, only the CO_2 and the H_2O detected between 200°C and 650°C were considered. The mass spectrometer signals of the CO_2 (44) and H_2O (18) were then integrated between the mentioned temperatures, and the ratio of these areas was considered to be proportional to the H/C atomic ratio of the coke deposit [18].

$$\frac{H}{C} \sim \frac{I_{18}}{I_{44}} \qquad \textbf{Equation 1}$$

In the previous equation, I44 represents the area measured for the CO_2 (m/z = 44) signal, and I18 the area corresponding to water (m/z = 18).

The nature of the coke was investigated by Raman spectroscopy. The analysis was performed on a Renishaw Raman spectrometer using an argon-laser focused on the sample by a microscope. Spent catalysts were analyzed in their extrudate form. The sample was cut with a scalpel along the transverse axis to obtain a flat cut that allows the analysis of the solid. Spectra of spent catalysts can often be compared to the spectra of graphite-like coke (peak at 1580 cm^{-1}) [25]. There are two graphite-like predominant bands. These bands are identified by group theory at 1580-1600 cm^{-1} (band G) and 1350-1400 cm^{-1}(band D1) [25]. They result from the vibration of C=C bonds of the coke in both perpendicular and plane directions, respectively.

The MoS_2 sheets were visualized and analyzed by transmission electron microscopy (TEM) with a JEOL JEM 2100F microscope. The samples were prepared in three steps. In the first step, the catalyst was ground to a fine powder. Then it was dispersed in ethanol in an ultrasonic bath, and two drops of the solution were deposited on a copper grid. Finally, the solvent was evaporated, and the sample was introduced into the microscope. The TEM images were recorded in bright field mode. The average dispersion of the MoS_2 particles was calculated from the slab length distribution, assuming a hexagonal shape of the particles [26]. The promoter segregation was investigated by TEM–EDX detection, leading to a Ni/Mo ratio calculated for about 25 particles.

Finally, evaluating the residual activities of the spent catalysts provides essential information on the catalyst deactivation state. In this case, the aim is to evaluate both the hydrogenating and isomerizing/cracking activities. Concerning the hydrogenating function, activity was evaluated via the conversion of toluene to hydrogenated products, following the protocol described elsewhere [27]. For the acidic function, the isomerizing/cracking activity was assessed via the hydroconversion of n-heptane to isomerization and cracking products using a testing protocol analogous to the one used for toluene hydrogenation. For both cases, the reaction is carried out in a fixed bed reactor in the presence of H_2S (generated by decomposition of DMDS) under hydrogen pressure. The operating conditions for each

experiment are presented in Table 5. Catalyst samples were sulfurized in situ at the beginning of the experiment, with the same feedstock and same operating conditions (T=350°C) as presented in Table 5, for 2 hours.

Table 5. Operating conditions of the catalytic tests with model molecules.

		Toluene Hydrogenation	n-Heptane Hydroconversion
Concentration of reactant	wt %/feed	20*	95.15
DMDS concentration	wt %/feed	6	4.85
P	MPa	6	6
LHSV	h^{-1}	2	4
T	°C	350	350/360/380
H_2/HC	NL/L	450	330

* in cyclohexane as solvent

Data interpretation: kinetic laws, deactivation parameter and H2 consumption

Deactivation was assessed by monitoring the evolution of the apparent kinetic constants for the target hydrocracking reactions, i.e., cracking, hydrodenitrogenation (HDN), aromatics hydrogenation (HDA) and hydrodesulfurization (HDS). These equations are based on the conversion of VGO ($370°C^+$) for cracking reactions and nitrogen, sulfur and aromatics for HDN, HDS and HAD, respectively. **Equation 2** shows the general expression to calculate the conversion. Along with this work, the results are given in terms of either global or first reactor properties. The term "global" is applied to reactor 1 and reactor 2 as a whole. Thus, for instance, the "global net conversion" is determined from the difference between the $370°C^+$ cut mass fraction at the first reactor inlet and the $370°C^+$ cut mass fraction at the second reactor outlet. Conversely, the "first reactor net conversion" is calculated through the difference between the $370°C^+$ cut mass fraction at the first reactor inlet and the $370°C^+$ cut mass fraction at the first reactor outlet. Some authors [16,28,29] have used power-law models to calculate these apparent kinetic constants for similar reaction systems. This type of expression was also used in this study for the sake of simplicity, although Langmuir-Hinshelwood-based models would be more appropriate for kinetics determination purposes. A first-order [17] kinetics was assumed for N-containing and aromatic molecules [30], i.e., for HDN and HDA, respectively (Equation **3**). An apparent reaction order of 1.2 for the S-containing molecules (Equation 4) was considered in the case of HDS. To determine the

apparent HDA kinetic constant, the amount of aromatic carbon was estimated through the n-d-M method according to the standard ASTM D3238.

$$\%\text{Net Conversion} = \left(\frac{x_{feed} - x_{product}}{x_{feed}}\right) * 100 \qquad \textbf{Equation 2}$$

Where x is either the 370+ mass fraction, the nitrogen, the sulfur or the aromatic carbon content.

$$k = \text{LHSV} * \ln(1 - \%\text{Net Conversion}/100) \qquad \textbf{Equation 3}$$

$$k_i = \frac{\text{LHSV}}{n-1}\left(\frac{1}{(C_s^{out})^{n-1}} - \frac{1}{(C_s^{in})^{n-1}}\right) \qquad \textbf{Equation 4}$$

Here n=1.2, C_s^{in}, and C_s^{out} are the feed and product concentration of sulfur.

Kinetics and deactivation were decorrelated through the fitting of an exponential decay function to the experimental data. An exponential decay function (Equation 5) was assumed for catalyst deactivation (φ), which depends on the deactivation constant (α) and time on stream (TOS) [9,28]. The deactivation constant was fitted to the experimental data of the cracking apparent kinetic constant evolution as a function of time.

$$k_{crack} = k_{crack}^{fresh} \exp(-\alpha * TOS) \qquad \textbf{Equation 5}$$

The hydrogen consumption was calculated from the experimental data by performing a global hydrogen balance (Equation 6). It was based on the elemental analysis of liquid streams and on gas chromatography. Hydrogen in gas compounds such as H_2S and light hydrocarbons (C_1 to C_6) was calculated from molar equivalents, and assuming all the

hydrocarbons to be paraffins. All the molecules measured by GC were assumed to be uniquely in the gas phase.

$$H_{cons} = H_{Liq}^{out} - H_{Liq}^{in} + H_{Light\ HC}^{out} + H_{H_2S}^{out} \qquad \textbf{Equation 6}$$

H_{cons} is the hydrogen consumption, H_{Liq}^{out} is the total amount of hydrogen contained in the hydrocracked liquid product, H_{Liq}^{in} is the total amount of hydrogen contained in the hydrotreated liquid feed, $H_{Light\ HC}^{out}$ is the amount of the hydrogen contained in light hydrocarbons and $H_{H_2S}^{out}$ is the amount of hydrogen contained as H_2S in the gas phase.

RESULTS

In this section, the results obtained during the screening of the operating conditions are presented first. The results of the final accelerated deactivation protocol are exposed afterward, together with the spent catalysts' characterization.

Variables screening experiment

The sequence of changes made in the operating conditions and the global net conversion evolution during variables screening are depicted in Figure 2 and Figure 3, respectively. The analysis of Figure 3 can be carried out by considering the influence of the operating conditions on catalyst activity, as well as on catalyst deactivation. We first focus on the impact of operating conditions on catalyst activity. The increase of temperature naturally favors conversion, which increases from 40 to 70%. The decrease of the H_2/HC ratio has a low impact on conversion, kept at an almost constant level of 30%. An increase of the LHSV translates into a lower residence time, which provokes a decrease in conversion up to 10%. Finally, the increase of the organic nitrogen content has practically no effect on conversion. This result was expected since the literature shows that as nitrogen level increases from zero, the conversion drops sharply until a certain nitrogen concentration, but then the loss of activity becomes less pronounced as nitrogen level increases [3]. During the hydrocracking

at 370°C of a hydrotreated VGO at different nitrogen levels, a conversion loss of around 60% was observed when nitrogen increased until 120 ppm. However, a loss of only 15% was observed beyond that concentration up to 600 ppm nitrogen.

From a deactivation point of view, a rapid drop in conversion is observed at the beginning of the experiment, under reference conditions. This result is consistent with the high activity of fresh catalysts that present a perfectly clean active surface. The temperature increase has a strong effect on catalyst deactivation, as conversion under reference conditions is reduced from 40 to 30%. The H_2/HC ratio does not affect catalyst deactivation, as the global net conversion remains at an almost constant value of 30%. LHSV strongly deactivates the catalyst, as conversion drops to 20% net conversion. Finally, organic nitrogen has no substantial effect on catalyst deactivation. An additional experiment was carried out to validate this result, as a totally deactivated catalyst could have masked the organic nitrogen impact on catalyst deactivation. Acridine and carbazole in a mass proportion of 1:3, respectively, were added to the feedstock to achieve a total organic nitrogen content of 300 ppm wt. Results are depicted in **Figure 4**. No significant impact of additional organic nitrogen is observed, either in terms of catalyst activity or catalyst deactivation. This observation consolidates the fact that, beyond 150 ppm wt., further increase of the organic nitrogen content does not practically affect activity, nor catalyst deactivation.

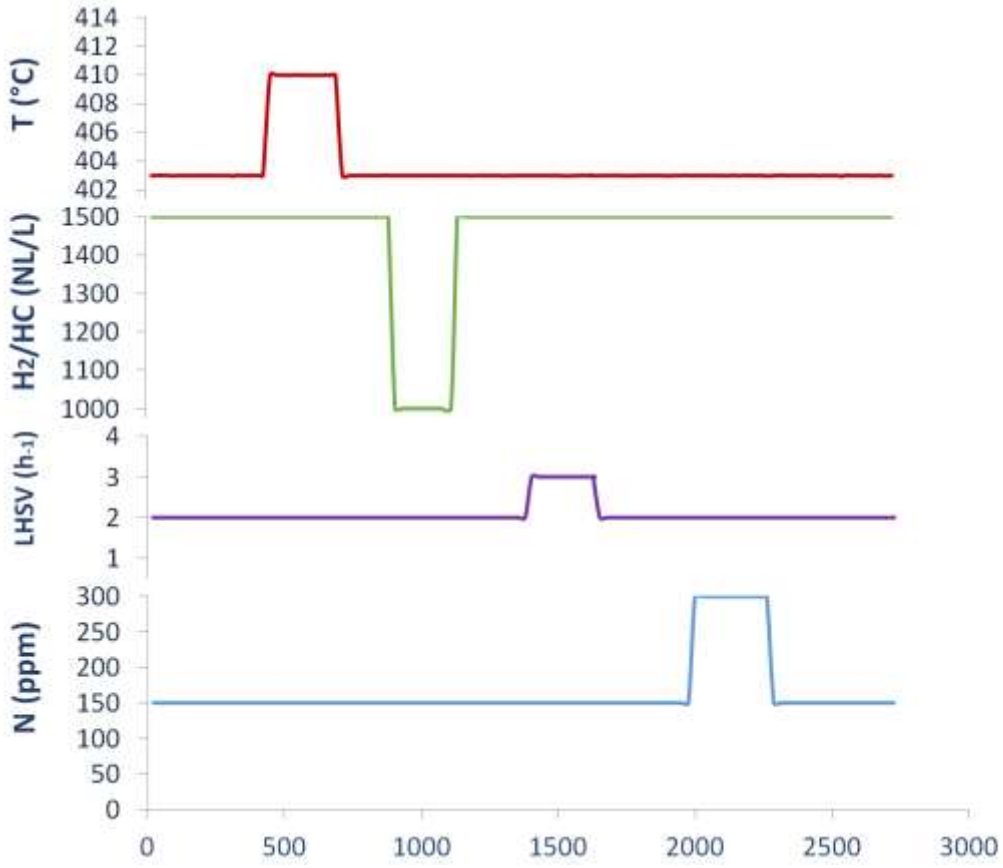

Figure 2. The sequence of changes made during the screening of the operating conditions.

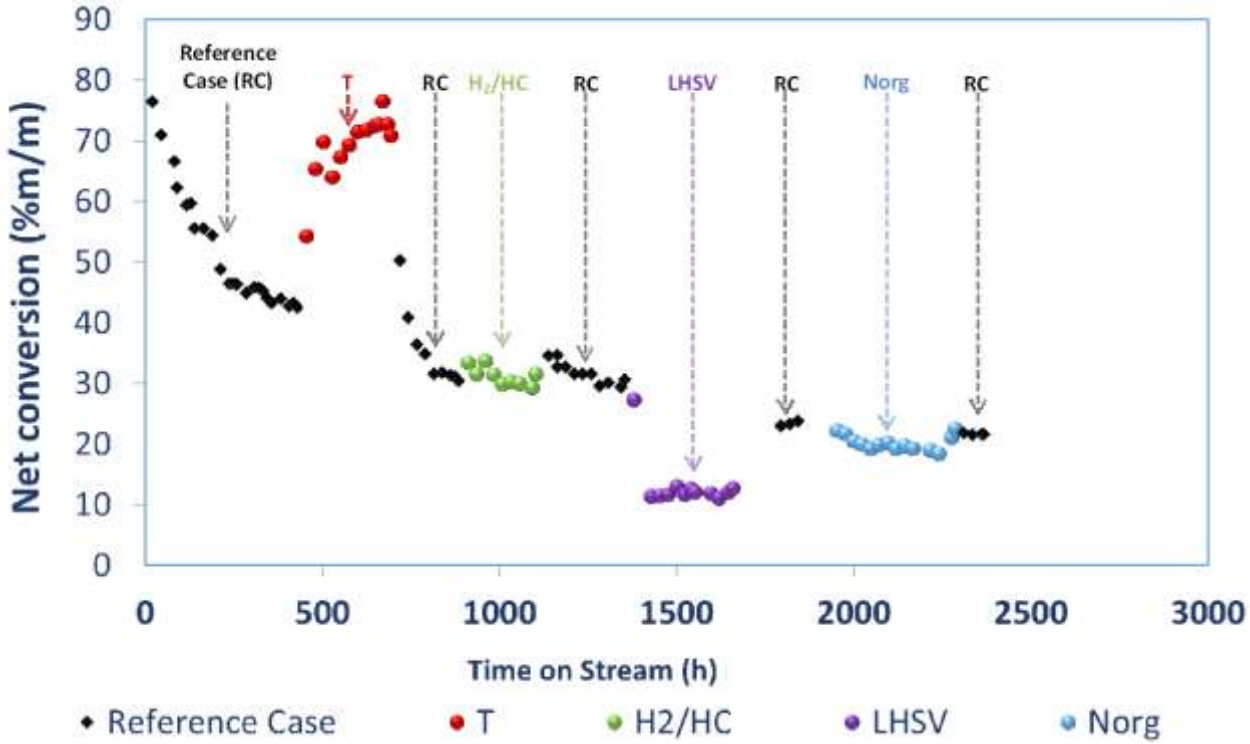

Figure 3. Net conversion as a function of time on stream, at the different operating conditions specified in Table 4.

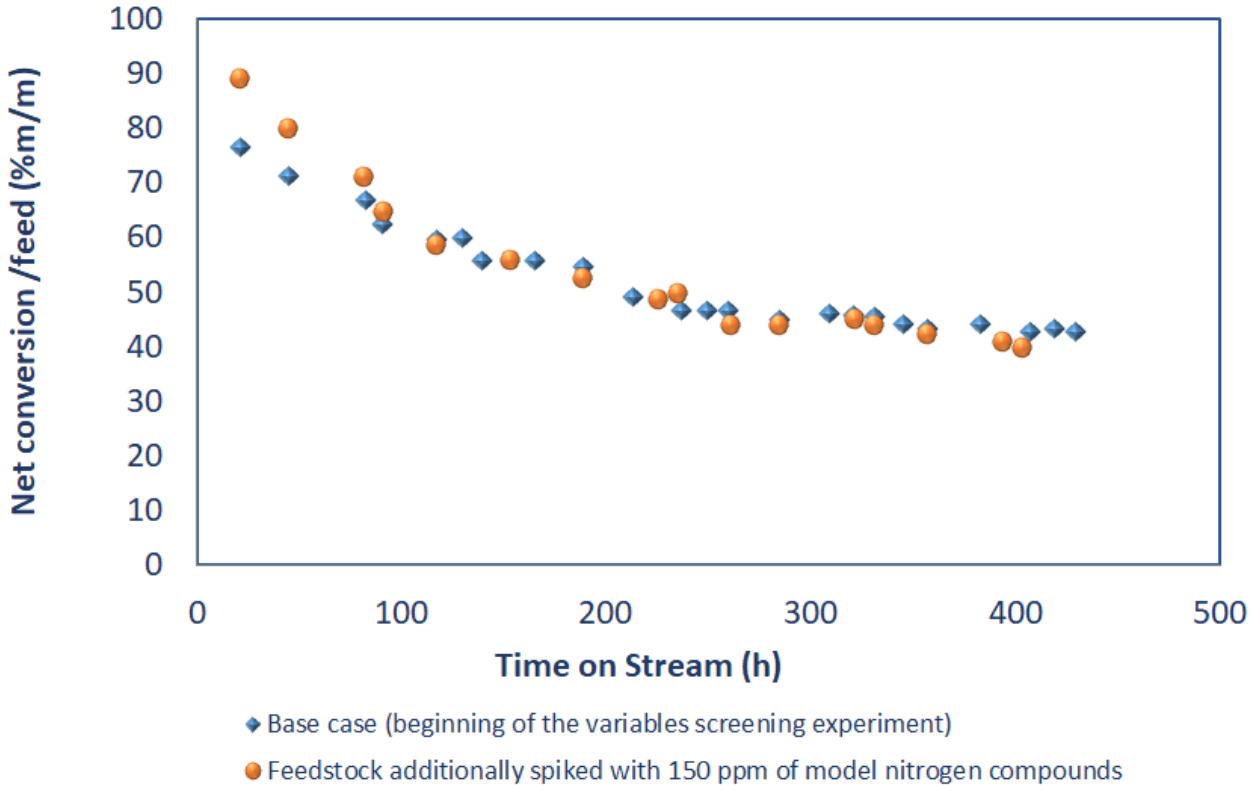

Figure 4. Effect of nitrogen content in the feedstock. Global net conversion evolution with time on stream and nitrogen content at the outlet of the reactors at the end of the experiment.

The evolution of the apparent kinetic constants of each key chemical reaction with time on stream is presented in the following sections, first for the whole system and then for the first reactor R1. These results quantify the effect of each variable on deactivation separately, so as to define the operating conditions for the accelerated deactivation protocol.

Evolution of kinetic constants with time for the whole system

The evolution of the global apparent kinetic constants of the relevant chemical reactions (cracking, HDN, HDCA, and HDS) with time on stream (TOS) is shown in **Figure 5**.

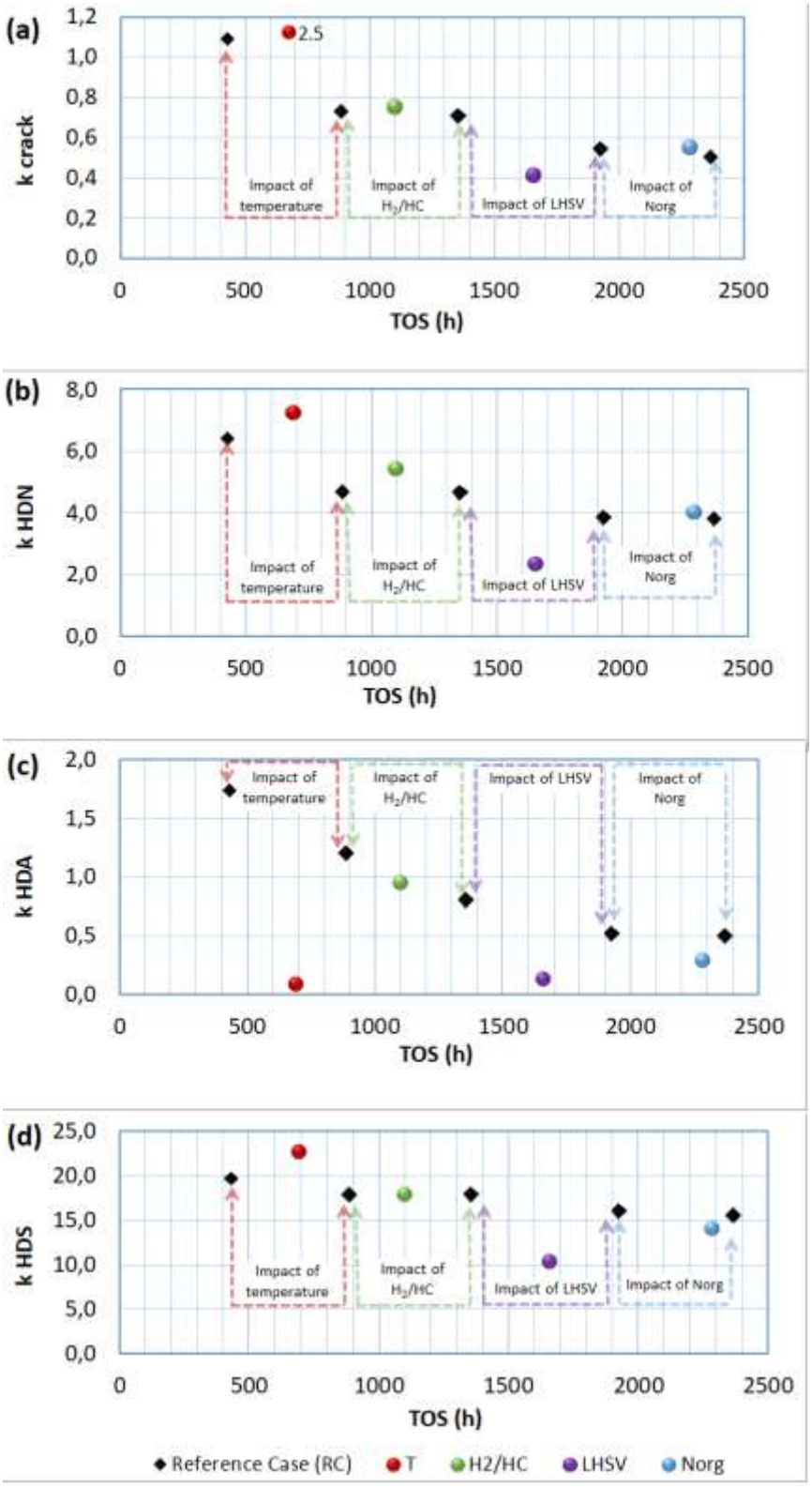

Figure 5. Apparent kinetic constants a) for cracking reactions, b) for hydrodenitrogenation reactions, c) for aromatics hydrogenation reactions, d) for hydrodesulfurization reactions at reference conditions and for each variable change specified in Table 4.

Reactivity

It is worth to comment on the effect of the operating variables on each chemical reaction rate (i.e. the colored points in **Figure 5**) before discussing deactivation. The impact of each operating variable on the HDN apparent kinetic constant is very similar to the one observed for the cracking function (**Figure 5**a vs b). The correlation between both apparent kinetic constants is shown in **Figure 6**. HDN reactions determine the residual organic nitrogen content. This has a strong repercussion on the cracking function of the catalyst through its inhibition [40]. A similar behaviour can be observed for both the HDA and the HDS apparent kinetic constants, except in the case of the effect of an increase of temperature on HDA. In fact, the related apparent kinetic constant approaches zero in that case. This can be attributed to the chemical equilibrium between aromatics and naphtenes, which is unfavourable at high temperatures. This observation is consistent with other works showing that HDA reactions are limited by chemical equilibrium at low pressure and high temperatures [32,33]

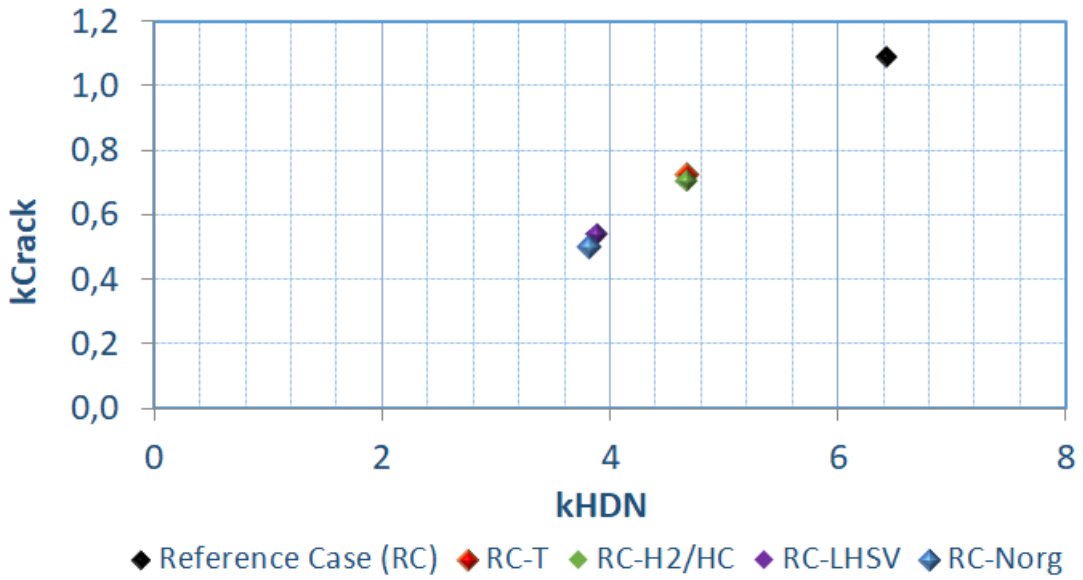

Figure 6. Correlation between hydrodenitrogenation and cracking kinetic constants.

Deactivation

Concerning deactivation, i.e. the activity difference at reference conditions after each variable change, the results are presented in Table 6. Temperature and LHSV are, by far, the variables having the strongest impact on catalyst deactivation. The deactivation mainly affects cracking, HDN and HDA reactions. The HDS reaction rate remains almost unchanged.

Table 6. Impact of variables on deactivation: extent of deactivation caused by each variable change.

$$100 - \frac{k_{ref\ case\ i}}{k_{ref\ case\ i-1}} * 100$$

	Cracking	HDN	HDCA	HDS
	%	%	%	%
Impact of Temperature	33	27	31	9
Impact of H_2/HC	3	0	33	0
Impact of LHSV	21	17	36	10
Impact of Norg	7	1	3	3

The data show that increasing temperature had the biggest impact on catalyst deactivation for every reaction. This result agrees with several studies in the literature claiming that coke precursors are formed faster and deactivate catalysts through carbonaceous compounds deposition at high temperatures [1,4,8,12,31]. The temperature excursion deactivated cracking, HDN, and HDCA reactions to roughly the same extent, whereas HDS was less affected.

Even if a higher hydrogen/hydrocarbon (H_2/HC) ratio is supposed to retard coke deposition due to the saturation of compounds involved in coke formation [3], the amplitude of the variation of this variable was not sufficient to observe any significant impact on deactivation. After the restoring of the reference conditions, all the apparent kinetic constants remained almost constant, except for HDA, which decreased by 33%.

The variable with the second-highest impact on deactivation was the space velocity. A higher space velocity lowers the residence time and, consequently, lowers the conversion of the different reactions. In the case of the HDN reactions, this reduction causes an increase in the nitrogen compounds concentration along the reactor. In contact with the catalyst, these

compounds can be adsorbed on the acid sites, thus neutralizing and leaving them unavailable for the VGO molecules to react. The adsorbed organic nitrogen compounds remain on the catalyst surface leading to coke formation due to coking reactions that are faster than the desorption of nitrogen-containing compounds [3]. When returning to the reference case conditions, this coke deposition reduces cracking reactions rate and conversion with respect to the values observed for the previous point made at the same conditions, as illustrated in **Figure 2** and **Figure 3**. There is also a reduction in the HDA reaction rate that increases aromatics concentration along the reactor. According to the mechanisms of carbenium ions proposed by different authors [1,34], when there is weak hydrogenation, aromatics can undergo addition, dehydrogenation, and hydrogen transfer reactions to grow into large polyaromatic molecules, i.e.,,, coke precursors.

The behavior of the HDS kinetic constant is particularly interesting. As mentioned before, the hydrotreating reactions are carried out on metal sulfide particles. However, **Figure 3** shows that the HDS kinetic constant remained nearly constant for all the reference points. In contrast, the HDN and HDA kinetic constants exhibit more important changes with TOS. This behavior can be explained, considering that desulfurization occurs through two different mechanisms, direct desulfurization (DDS) and pre-hydrogenation (HYD) [4,6]. The catalytic sites responsible for each one of these mechanisms are different. Some studies [35,36,37] have established that sulfur vacancies promote the DDS pathway, and hydrogenation is promoted either by the so-called Brim sites [35,38] or by the acidic SH groups [39]. Despite the current controversy over these sites, there is an agreement concerning the strong inhibition of the HYD pathway by basic nitrogen compounds [38], consistent with the observed decrease of the HDA and HDN kinetic constants upon deactivation by organic nitrogen compounds in the feed. The existence of an alternative reaction pathway, the DDS, for HDS, allows explaining why this particular chemical reaction is less affected.

The evaluation of the impact of the different operating variables on deactivation allows the following ranking to be established: $T>LHSV>H_2/HC>N_{org}$. The determination of the

deactivation parameters for the cracking function as well as the hydrogen consumption evolution consolidates this ranking, as shown hereinafter.

The ratio of the deactivation rate coefficients for cracking reactions is presented in **Table 7**. The results confirm that the variables impact on the deactivation rate at the evaluated conditions, follows the order mentioned previously.

Table 7. Impact of variables on the deactivation rate for cracking reactions.

	$\alpha_{ref\ case\ i} / \alpha_{ref\ case\ i-1}$
	Cracking
Impact of Temperature	3.0
Impact of H_2/HC	0.3
Impact of LHSV	2.3
Impact of Norg	0.0

Finally, **Table 8** shows the hydrogen consumption for each point of the variables screening. The data were consistent with the evolution of the cracking kinetic rates. The higher the kinetic constant, the higher the hydrogen consumption. This result agrees with the hydrocracking stochiometry, which predicts the consumption of one H_2 molecule per cracking reaction.

Table 8. Hydrogen consumption and apparent kinetic constant for cracking reactions.

	Condition	H_{cons}	k_{Crack}
		Nm^3/m^3	
2	Impact of Temperature	60	1.09
4	Impact of H_2/HC	47	0.73
6	Impact of LHSV	45	0.71
8	Impact of Norg	41	0.54

Evolution of the kinetic constants with time for the first reactor

The analysis of the effluent of the first reactor allows pushing the interpretation of the data a little bit further. **Figure 7** shows a comparison between the apparent kinetic constants in the first reactor and in the whole system for cracking and HDN reactions. HDA reactions were not considered since the respective kinetic constants were negligible.

Reactivity

The effect of the different operating variables on each reaction rate is not discussed here as it is quite similar to the one observed for the whole system. The apparent kinetic constants of the first reactor are lower than the corresponding global values. This is probably due to the higher organic nitrogen content in the first reactor, which strongly inhibits chemical reactions.

Deactivation

The cracking apparent kinetic constant for reactor R1 remained nearly unchanged for all the reference conditions, whereas the global value displayed a decrease, as discussed in the previous section. The HDN kinetic constant of the first reactor followed the same trend as the global HDN constant. The absence of further deactivation of the cracking function in the first reactor, despite a systematic deactivation of HDN, can be explained by the saturation of the inhibition effect at high organic nitrogen concentration. This is in agreement with the conclusions from the experiment carried out at a higher organic nitrogen content.

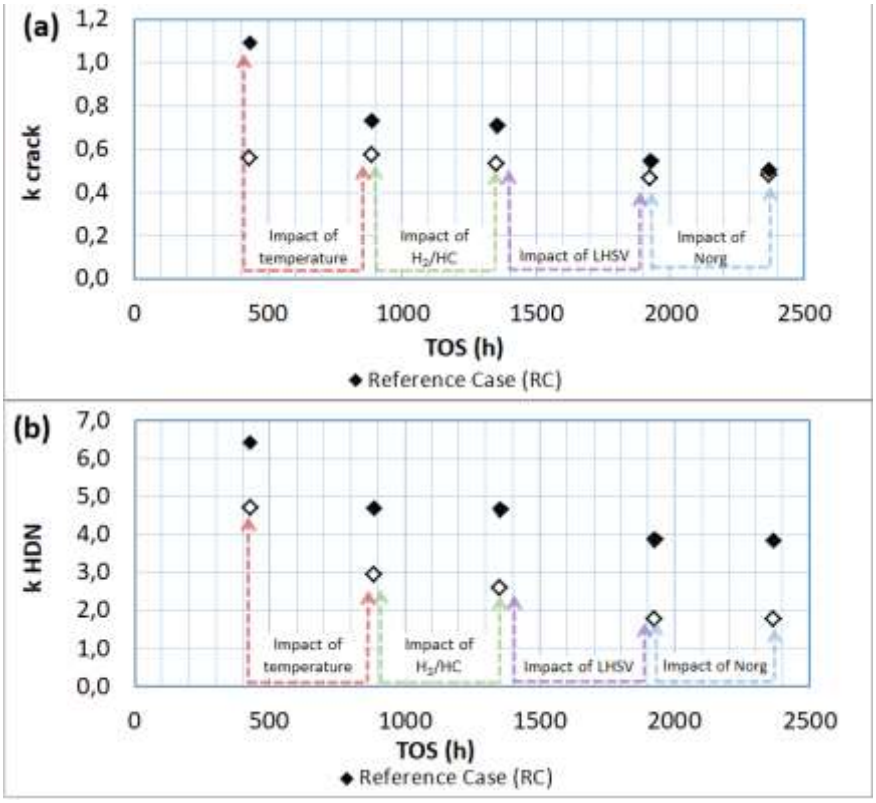

Figure 7. Kinetic constants of a) Cracking reactions b) HDN reactions at reference conditions before and after each variable change. Full symbols=whole reactor system, open symbols=first reactor.

In conclusion, the variable screening experiment showed that the two variables, which had by far the strongest impact on deactivation, were temperature and space velocity. Therefore, a high temperature associated with a high space velocity were chosen for the accelerated deactivation protocol. The highest LHSV which was feasible on the testing unit was 3 h^{-1}. At this LHSV, the highest possible temperature, which avoided full conversion of the 370°C^{+} fraction was about 418°C.

Accelerated deactivation protocol

Evolution of net conversion and apparent kinetic constants over time

The catalyst was subjected to the accelerated deactivation conditions for one month. The evolution of the global and first reactor net conversions over time is presented in **Figure 8**. After the stabilization time, global conversion decreased by about 20%. Industrial conversion losses are considerably lower, i.e., around 5%/month. The main loss of activity occurred in the first 7 days; after this time, the decline rate was lower until conversion reached a pseudo-steady state. The conversion evolution with time on stream followed the trend usually obtained during coke formation on hydroprocessing catalysts [3,9]. During industrial catalyst deactivation through coking, coke is rapidly formed in the initial stages of the operation; then, the coke level reaches a near steady-state [6]. The conversion in the first reactor remained constant after the stabilization time, as already observed during the variables screening experiment.

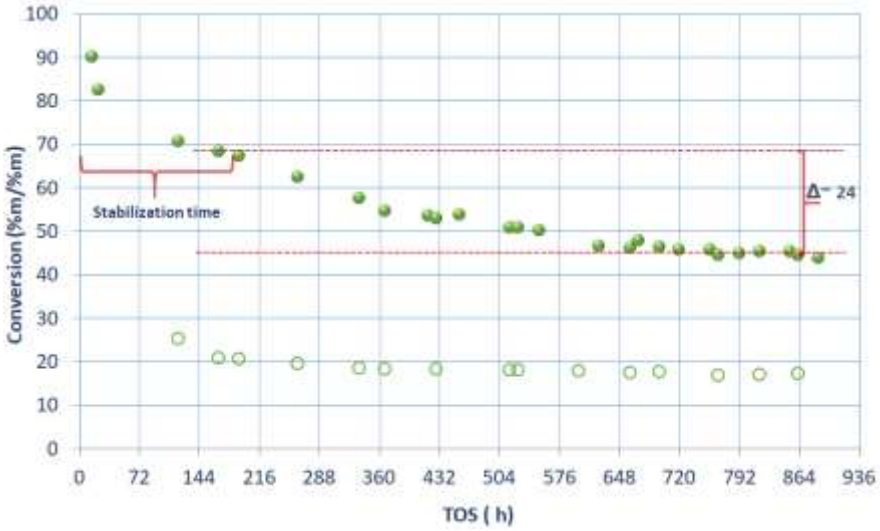

Figure 8. Evolution of the global and first reactor net conversion with time on stream with the accelerated deactivation protocol (T=418°C, P=14 MPa, LHSV=3h^{-1}, H_2/HC= 1500 NL/L). Full symbols=Total effluent, open symbols=First reactor effluent.

The evolution of cracking and HDN apparent kinetic constants over time is presented in **Figure 9**. The results show a reduction of around 40% and 25% in the global cracking and HDN reaction rates, respectively. Hence, the acid function undergoes a higher deactivation than the metal function. The cracking and HDN rate constants in the first reactor remained constant during the whole test, confirming that different mechanisms took place in each reactor.

The obtained results allow us to partially decorrelate the cracking function deactivation from the HDN conversion loss. Indeed, the HDN apparent kinetic constant reached a pseudo-plateau after around 144 h of operation, whereas the cracking apparent kinetic constant continuously decreased until 500 h of operation. Thus, the cracking activity loss was not entirely explained by inhibition due to a progressive increase in the organic nitrogen content, i.e. an indirect consequence of the deactivation of the HDN activity. Although this indirect effect certainly contributes to the deactivation of cracking, a direct deactivation mechanism of the acid sites must exist in parallel.

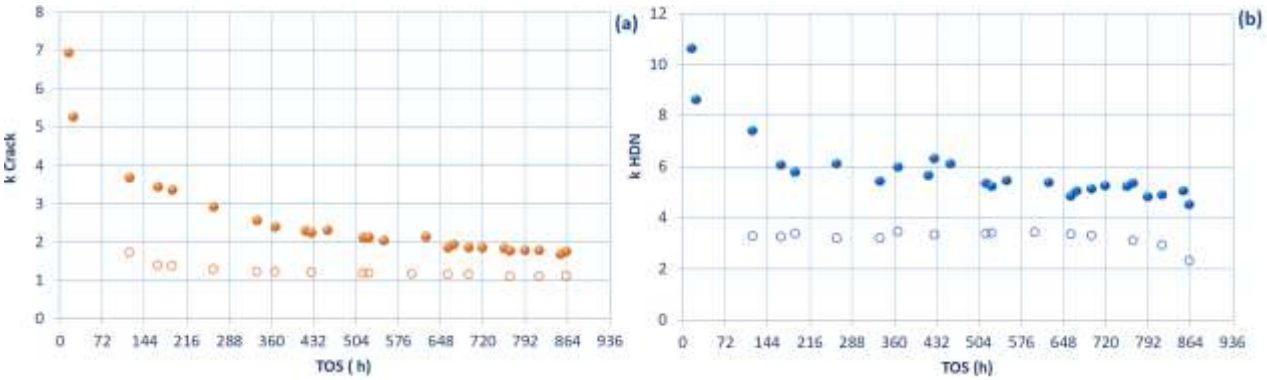

Figure 9. Evolution of apparent kinetic constants with time on stream during the deactivation test, a) for cracking reactions, b) for hydrodenitrogenation reactions. Full symbols=whole reactor system, open symbols=first reactor .

Spent catalysts characterization

This section presents the characterization results of the spent samples from the accelerated deactivation procedure. Samples were drawn from the first reactor inlet (Bed inlet) and from the second reactor outlet (Bed outlet) to understand the effect of reactor location on deactivation. These results are compared to the characterization results obtained for the samples from the reference test, described in section 0, to assess the extent of deactivation. Finally, some characterization results related to industrial spent catalysts are exposed for the qualitative validation of the experimental procedure's representativeness.

Elemental analysis

Results from the elemental analysis are shown in Table 9. As expected, the catalyst from the accelerated deactivation experiment has a higher carbon content than the catalyst obtained from the reference test. The carbon content of industrial spent catalysts was even higher. Regarding the effect of reactor location, the carbon content of the spent catalyst at the reactor outlet was higher than at the reactor inlet.

The N/C ratio of the coke decreases along the reactor, in agreement with the organic nitrogen evolution as a reactor location function.

Table 9. Characterization of spent catalysts: Surface area (S), total pore volume (V), micropore volume (μV) and hysteresis area of the spent catalyst relative to the fresh catalyst and carbon content of the spent catalysts.

Sample	Carbon content	S/S_{fresh}	V/V_{fresh}	$\frac{\mu V}{\mu V_{fresh}}$	$\frac{HA_{Spent}}{HA_{Fresh}}$
	(% wt)	(%)	(%)	(%)	
Reference Test - Bed In	5.1	92	85	84	1.1
Reference Test - Bed Out	5.4	95	86	87	1.1
Deactivation Test - Bed In	6.2	86	81	65	1.2
Deactivation Test - Bed Out	8.1	71	71	60	1.4
Industrial Spent Catalysts	10 -15	65 – 85	60 - 85	65-78	1.4-1.6

Textural analysis

The porosity of the spent catalysts from the accelerated deactivation procedure was analyzed via the nitrogen adsorption-desorption isotherms. Coke caused a decrease in pore volume, which was accompanied by a decrease in surface area (Table 9). The accelerated deactivation procedure provoked higher surface area losses (S) and pore volume (V) than the reference test. These relative losses were within the range typically observed for industrial spent catalysts. A more pronounced decrease of surface and pore volume was observed at the bed outlet, in agreement with the higher carbon content at this location.

The pore size distributions of the different catalyst samples, measured by nitrogen desorption isotherms, are shown in **Figure 10**. Note that in this figure, the mesopore distribution is the pore distribution of the carrier and not of the USY crystals. The pore size distribution of the deactivated samples always remained similar to the one determined for the fresh catalyst, except for a shift towards smaller pores. This phenomenon was very pronounced for the deactivated solids from the accelerated deactivation protocol and even more for the bed outlet sample, consistent with higher carbon content in this location. Furthermore, the loss of micropore volume (μVol) follows the same tendency as global volume loss (Table 9). Both facts suggest that the deposition of coke seems to be homogeneous in all pores.

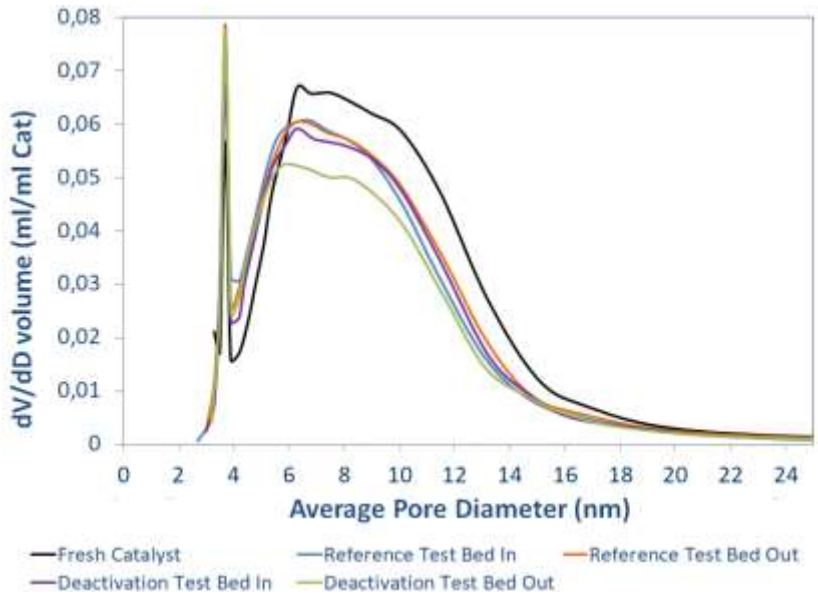

Figure 10. Catalyst pore distribution (Nitrogen desorption isotherm).

An approach based on the ratio of the hysteresis area of the spent catalyst with respect to the hysteresis area of the fresh catalyst was developed by Sámano et al. [41]. The authors established this ratio as a semi-quantitative analysis to evaluate the extent of catalyst deactivation. **Table 9** indicates that the ratio of areas is higher for samples from the accelerated deactivation test than for samples from the reference test, as expected. Results also showed lower values for the spent samples from the first reactor inlet than for the reactor outlet, in accordance with the previous results. The obtained values for the pilot deactivated samples were close to the magnitude observed for industrial spent catalysts.

TGA analysis

The spent catalyst samples were characterized by TGA analysis to compare the nature of coke deposits. The first time-derivative of weight loss as a temperature function is illustrated in **Figure 11** for bed inlet and bed outlet samples from the deactivation test.

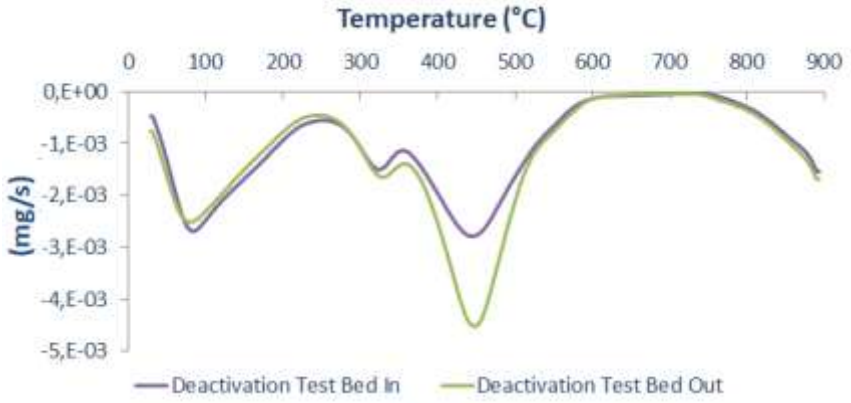

Figure 11. TGA profiles of bed inlet and bed outlet samples from the deactivation test.

The first peak around 100°C corresponds to H_2O desorption, whereas the second one (280-330°C) and the third one (350-550°C) correspond mainly to SO_2 and CO_2 releases, respectively. Consequently, and in agreement with other studies [21,42,43], it is concluded that the deposit on the catalyst is composed mainly of carbon, whereas the SO_2 detected can be attributed to the molybdenum sulfide.

In general, the quantity of coke deposit is related to the intensity of the third peak (350-550°C) [6, 34]. The TGA results (**Table 10**) confirm the elemental analysis; The coke content was higher for the spent samples coming from the bed outlet of the deactivation test.

The temperature related to the maximum weight loss is an indicator of the nature of coke. The coke structure is expected to be more graphitic, hence more difficult to combust, at higher values of maximum weight loss temperature. The peak temperatures indicate that catalyst samples from the bed outlet (peak at 450°C) contained a slightly more graphitic coke than the spent solids from the bed inlet (peak at 445°C). The coke can be further characterized by determining its H/C ratio, which is proportional to the ratio of the CO_2 (44) and H_2O (18) mass spectrometer signals, I_{18}/I_{44}. As was mentioned in section 2.3.4 only the CO_2 and the H_2O detected between 200°C and 650°C were considered. The lowest I_{18}/I_{44} ratio of the coke deposited, and then the higher coke aromaticity was found for the industrial samples, followed by the bed outlet and the bed inlet samples from the deactivation test. The reference test samples presented the highest values, that is, the lowest coke aromaticity.

Regarding bed location, the aromatic character increased from the first reactor inlet towards the second reactor outlet.

Table 10. Estimation of CO_2 mass loss and H/C ratio of the coke deposit from ratio I18/I44 from TGA profiles for different spent catalysts.

Sample	CO_2 mass loss (wt %)	I18/I44
Reference Test-Bed In	8.0	4.3
Reference Test-Bed Out	8.3	4.3
Deactivation Test- Bed In	9.1	3.4
Deactivation Test-Bed Out	11.0	2.1
Industrial Spent Catalysts	13-16	0.5-0.9

Raman analysis

The differences in aromaticity of the coke produced during the reference and deactivation experiments and some industrial cycles were confirmed by Raman spectroscopy. The spectra are showed in **Erreur ! Source du renvoi introuvable.**The reference test samples present high fluorescence, showing very noisy spectra. It indicates that the carbonaceous deposit was very poorly organized. In contrast, the spectra for the deactivation test and industrial spent samples were well defined. Hence, the carbonaceous deposit had a more organized structure in these cases. In fact, the two prominent peaks (1330 cm^{-1} and 1600 cm^{-1}) identified in the spectra are typically found in the case of a graphitic coke-type [24].

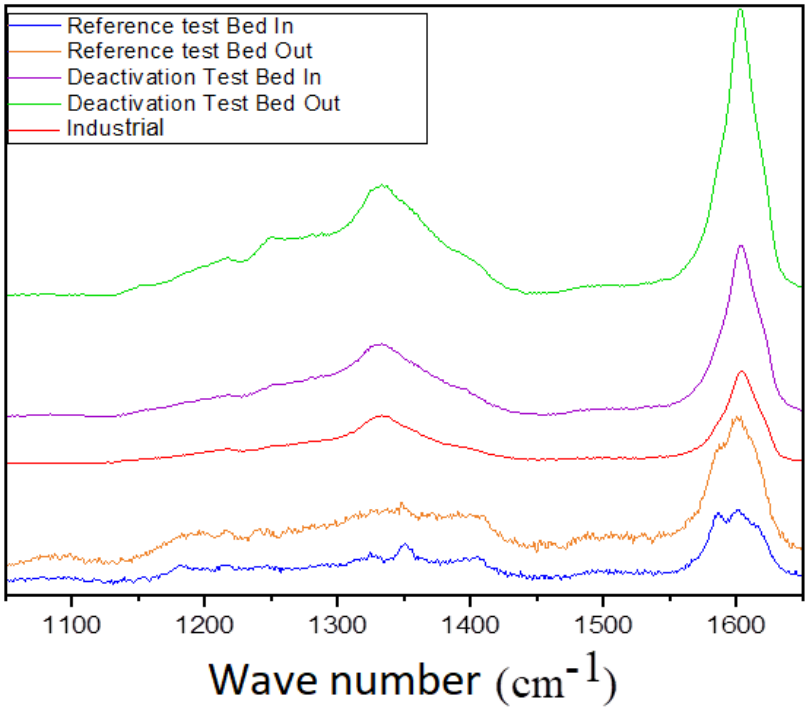

Figure 12. Raman spectra of spent catalysts from the reference test, the deactivation test and industrial cycles.

TEM/EDX analysis

TEM/EDX analysis were performed on spent samples from both the reference and the deactivation experiments. Morphology of the MoS_2 slabs and Ni/Mo ratio are presented in **Table 11**. The MoS_2 slabs for the deactivation test samples are between 10 and 25% longer than the reference test samples, whereas the dispersion values are very close. These results indicate a slight sintering of the MoS_2 slabs under severe conditions during the deactivation test. Finally, a significant nickel depromotion is observed for the deactivation test samples. The related Ni/Mo ratio is about 40% lower than in the reference test samples.

Table 11. Average slab length and dispersion measured by TEM and Ni/Mo ratio in MoS_2 particles measured by EDX.

	Slab length (nm)	Dispersion	Ni/Mo
Reference test bed in	**3.7±1.4**	**0.24**	**0.37±0.18**
Reference test bed out	**3.8±1.5**	**0.23**	**0.35±0.12**
Deactivation test bed in	**4.3±1.7**	**0.22**	**0.19±0.11**
Deactivation test bed out	**4.6±2.2**	**0.18**	**0.23±0.12**

Model molecule experiments

The residual catalytic activities of the different spent samples were evaluated through specific experiments with model molecules. The hydrogenation of toluene provides

information on the residual metal sites of the spent catalysts. The residual activity of the acid function is assessed through the n-heptane hydrocracking. The results are represented in **Figure 13**, which includes data related to the fresh catalyst. All spent catalysts present lower metallic and acid activities than the fresh catalyst, as expected. The deactivation test samples exhibit similar residual activities compared to the industrial samples and lower residual activities than the reference test samples.

The toluene conversion of the deactivation test samples was around 36% lower than the reference test samples. As mentioned above, the MoS_2 slab depromotion was 40% on average. According to previous works [44], there is a roughly linear correlation between the catalyst promoter content (Ni) and the hydrogenating activity. Hence, the loss of the hydrogenating activity can be mainly attributed to catalyst depromotion in that particular case. Furthermore, concerning the location impact on deactivation, spent samples from the second reactor exhibited slightly lower conversions in the hydrogenation of toluene than samples from the first reactor.

The loss of conversion for the fresh catalyst is much more pronounced in the n-heptane hydrocracking case (see **Figure 13** b vs. a). Thus, coke deposits seem to be preferentially located on the acid sites of the spent catalysts. Concerning reactor location, samples from the second reactor outlet exhibit slightly higher conversions than spent solids from the first reactor inlet. Consequently, the acid sites remained more active in the second reactor than in the first one, despite a higher carbon content and a higher aromatic character of the coke.

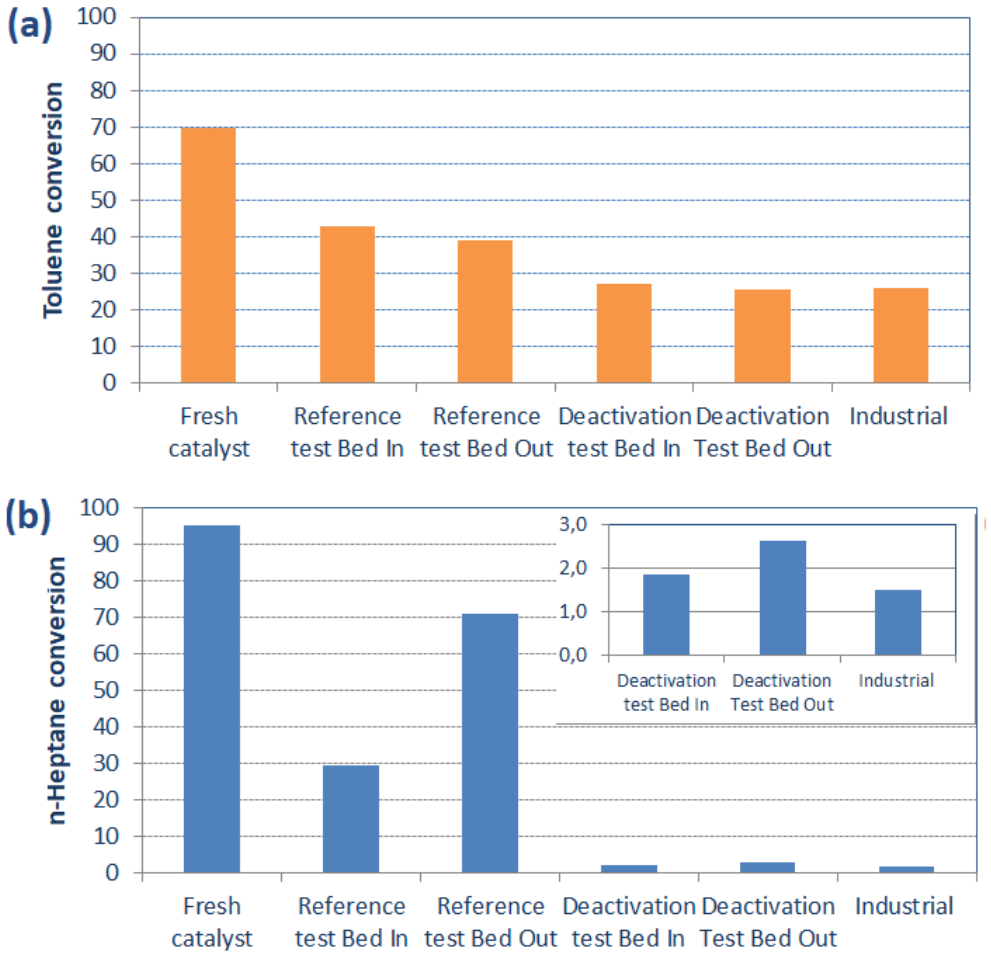

Figure 13. Catalytic activity evaluated by model molecules catalytic tests for the reference and the deactivation tests samples and some spent industrial catalysts. a) Hydrogenation of toluene, b) Isomerization/cracking of n-heptane at 360°C.

The selectivity towards i-heptane formation (the primary product) in the n-heptane hydrocracking experiment is illustrated in Figure 14 as an n-heptane conversion function. The selectivity towards the production of cracked products, C_3+C_4, naturally presents the opposite trend. The i-heptane selectivity, compared at the same conversion level, can be considered as an indicator of the residual metal/acid balance [45,46]. High selectivity is a sign of high hydrogenating activity as compared to the acid sites. A low i-heptane selectivity means that the acid sites are ill-balanced by the hydrogenating sites.

The i-heptane selectivity was higher in the case of the deactivated samples than the samples from the reference test as well as to the fresh catalyst. This is coherent with the previously described toluene hydrogenation and n-heptane hydroconversion activities. Indeed, these results show that the acid function underwent a much more severe deactivation than the

hydrogenation function for the deactivated catalysts. This positively influences the metal/acid balance, leading to an increase in the i-heptane selectivity. Regarding reactor location, in agreement with previous considerations, the selectivity to i-heptane was higher for spent samples from the first reactor.

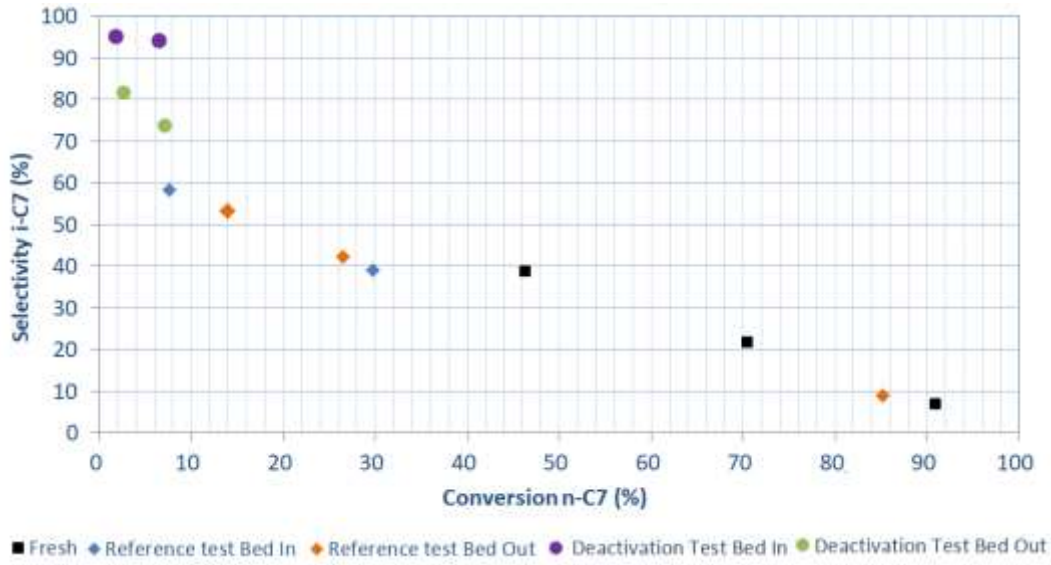

Figure 14. n-heptane hydrocracking experiment. Selectivity to i-C7 Vs. conversion n-C7.

RESULTS DISCUSSION

Considerations about the deactivation phenomena are given in this section, with a special focus on the main mechanisms leading to hydrocracking catalyst deactivation with real feedstocks.

Organic nitrogen plays a key role in the deactivation phenomena. Organic nitrogen compounds are rapidly adsorbed on the catalyst acid sites [2,3] due to their basic character. This adsorption firstly leads to acid site inhibition through neutralization and, subsequently, to an irreversible deactivation by coke deposits. These deposits are produced by the reaction between adsorbed nitrogen species. This result is in agreement with the decrease of the coke's N/C ratio along with the system (from 0.035 at the bed inlet to 0.025 at the bed outlet). Both inhibition and coking lead to the loss of cracking activity [34].

One of the issues related to bifunctional catalyst deactivation in this particular case is to decorrelate the cracking function loss of activity from the metal function's deactivation. In fact, the latter leads to a decrease in the HDN reaction rate. Thus, more nitrogen compounds are available to be adsorbed on the acid sites, resulting in a possible increase in acid function inhibition. Consequently, it is difficult to conclude if the cracking activity loss is simply due to further inhibition due to the increase of the nitrogen species concentration or other mechanisms such as coking by aromatics. The results obtained from the accelerated deactivation protocol (**Figure 9**) revealed that the cracking reaction rate continuously decreases even if HDN conversion remains almost unchanged. Moreover, the experiments performed with model molecules (**Figure 13**) showed an almost complete deactivation of the acid sites. Both findings indicate that the deactivation of the cracking function can be attributed to both inhibition by nitrogen species (which increases due to the deactivation of HDN) and coking of the acid sites.

The considerations made in the previous two paragraphs allow concluding on the mechanisms that lead to the deactivation of the acid sites. It is suspected that the very strong interaction of the organic nitrogen compounds with the acid sites may be at the origin of the coke formation. The N/C ratio values of the spent catalyst samples reinforce this hypothesis. These values are 0.035 mol/mol and 0.025 mol/mol for the bed inlet and outlet samples, respectively. This ratio is similar to the one related to typical organic nitrogen compounds in vacuum gas oils (molecules containing 20 to 40 carbon atoms and one nitrogen atom). Thus, an important proportion of coke originates from these nitrogen species, especially in the bed inlet samples. The higher amount of coke with a lower N/C ratio for bed outlet samples suggests that there might also be a contribution of aromatic compounds to the coke generation in the second reactor.

The effect of reactor location on the extent of the catalyst acid function deactivation is, once again, deeply linked to the organic nitrogen concentration evolution along the reactor. The bed inlet (and the first reactor as a whole) is exposed to a high concentration of organic

nitrogen, which leads an almost full inhibition of the cracking function in R1; the 370°C+ conversion can be attributed to hydrogenation and dealkylation reactions. This explains why the conversion in R1 remains constant after an initial stabilization period of ~150 h. In the second reactor, where the nitrogen inhibition was lower, a progressive loss of the cracking activity was observed before establishing a pseudo-plateau after ~500 h.

The spent samples characterization results agree well with the explanations given in the previous paragraph. The carbon content of the deactivated catalyst samples increases along the reactor, which is attributed to the inverse trend observed for the organic nitrogen concentration. In fact, the preferential adsorption of nitrogen compounds on acid sites inhibits polymerization of the dehydrogenated intermediates on metal sites, thus reducing the coke production rate. The textural properties show a higher loss in both BET surface and total volume related to spent solids from the second reactor.

The toluene hydrogenation test (Figure 13) showed a slightly higher residual hydrogenation activity for first reactor samples. This is contrary to the trend of the HDN kinetic constants in the pilot experiments, which exhibited a lower value in the first reactor (**Figure 7**, **Figure 9**). To explain this behavior, it is important to have in mind that the performance (kinetic constant) reflects both the inhibition and the permanent deactivation taking place over time on stream during the experiments. Model molecule catalytic tests are carried out on spent catalyst samples previously washed (see Section 2.3.5). As a result, these experiments display the residual activity due to the permanent catalyst deactivation exclusively. The extent of metal activity loss was assessed to 65%. This activity loss was mainly attributed to the significant observed Ni depromotion (**Table 11**). This depromotion reaches a value of 40% in the MoS_2 slabs of the spent catalysts from the accelerated deactivation procedure.

Finally, evaluating the ratio between available metal and acid sites allows concluding on the coke type as a function of reactor location. In fact, a difference in the relative rate at which each function is deactivated along the reactor induces a modification of the metal/acid sites'

ratio (M/A). Thus, the ratios related to deactivated and to the fresh catalyst samples are expected to be different, as illustrated via the i-heptane selectivity in **Figure 14**. According to the i-heptane selectivity, the (M/A) ratio is lower for spent samples at the bed outlet spent samples than for the bed inlet. This can explain the higher amount of coke in the second reactor and its more aromatic character (lower H/C ratio, **Table 9** and **Table 10**). Indeed, since the number of available metal sites is lower in the second reactor, the intermediate unsaturated coke precursors species produced on the acid sites undergo polymerization reactions before being hydrogenated.

CONCLUSIONS

- An accelerated deactivation protocol at the pilot plant scale was developed to study the hydrocracking catalyst deactivation phenomena in a short period of 30 days. From textural, elemental, thermogravimetry analysis as well as from the evaluation of the residual activities by model molecules tests, it is concluded that this protocol generates spent catalysts, which are very similar to industrial spent catalysts. This methodology allows a representative, fast and insightful way to evaluate the deactivation phenomena for hydrocracking catalysts. It can be used to evaluate the potential of a feedstock or certain operating conditions to coke and deactivate and compare different catalytic formulations from a stability point of view.

- The organic nitrogen content of the feedstock to the hydrocracking process is determinant in catalyst deactivation. The basicity of these compounds explains their strong adsorption on the acid sites (initial inhibitory effect), leading to the formation of coke deposits, which deactivate the catalyst acid function permanently. In contrast, nitrogen compounds have just an inhibitory effect on the metal function. The organic nitrogen impact on the reaction rates follows this order: Cracking>>HDN>HDCA>HDS. The HDS activity is less affected as desulfurization

can proceed via direct desulfurization (DDS), which does not rely on hydrogenation sites, which are inhibited by nitrogen.

- The deactivation of the metal function is mainly due to nickel depromotion; it reduces the hydrogenation activity by about 40%. The deactivation of the cracking function is much more significant. Due to two different mechanisms, the direct poisoning of the acid sites by the organic nitrogen compounds from the feed and an indirect consequence of the decreased HDN activity leads to a progressive increase of the average organic nitrogen concentration in the reactor during the time on stream. This increase in inhibition is mainly observed at reduced organic nitrogen contents, conditions at which these species do not fully cover the acid active surface.

- The coke composition analysis suggests that an important proportion of the coke originates from the organic nitrogen species. However, as the HDN is carried out along the reactor and nitrogen is removed, other mechanisms, like aromatic coke formation, start to play a more important role in catalyst deactivation.

- The balance in the ratio of the metal/acid sites determines the amount and the type of formed coke. The lower the ratio, the lower the hydrogenation of intermediate unsaturated coke precursors species produced in the acid sites, and consequently, the higher the coke production rate. A lower metal/acid balance also leads to coke presenting a lower hydrogen content and, as a result, a more aromatic (less reactive) structure. Since the metal/acid balance decreases from bed inlet to bed outlet (due to less inhibition by organic nitrogen at the bed outlet), the bed outlet contains a higher amount of coke, which is more aromatic.

Funding: This work was supported by IFPEN Energies Nouvelles and ECOPETROL.

References

[1] Scherzer J, Gruia AJ. Hydrocracking science and technology. New York: Marcel Dekker; 1996.

[2] Furimsky E, Massoth F. Deactivation of hydroprocessing catalysts. Catalysis Today 1999;52:381–495.

[3] Sau M, Basak K, Manna U, Santra M, Verma RP. Effects of organic nitrogen compounds on hydrotreating and hydrocracking reactions. Catalysis Today 2005;109(1-4):112–9. https://doi.org/10.1016/j.cattod.2005.08.007.

[4] Furimsky E (ed.). Catalysts for upgrading heavy petroleum feeds. Amsterdam: Elsevier; 2007.

[5] Vogelaar BM, Eijsbouts S, Bergwerff JA, Heiszwolf JJ. Hydroprocessing catalyst deactivation in commercial practice. Catalysis Today 2010;154(3-4):256–63. https://doi.org/10.1016/j.cattod.2010.03.039.

[6] Toulhoat H, Raybaud P (eds.). Catalysis by transition metal sulphides: From molecular theory to industrial application. Paris: Éd. Technip; 2013.

[7] Dujardin O. Étude Des Phénomènes De Desactivation. Paris: Université Pierre et Marie Curie; 1992.

[8] Moulijn J.A, van Diepen A.E, Kapteijn F. Catalyst deactivation: is it predictable? What to do? Applied Catalysis A: General 2001(212):3–16.

[9] Rashidzadeh M, Ahmad A, S. Sadighi. Studying of Catalyst Deactivation in a Commercial Hydrocracking Process (ISOMAX). Journal of Petroleum Science and Technology 2011;1(1):46–54.

[10] Hydrocarbon Publishing Company. Worldwide Refinery Processing Review 2017(2Q).

[11] S.T. Sie. Consequences of catalyst deactivation for process design and operation. Applied Catalysis A: General 2001(212):129–51.

[12] Bartholomew C. Mechanisms of catalyst deactivation. Applied Catalysis A: General 2001(212):17–60.

[13] Argyle M, Bartholomew C. Heterogeneous Catalyst Deactivation and Regeneration: A Review. Catalysts 2015;5(1):145–269. https://doi.org/10.3390/catal5010145.

[14] Tanaka Y, Shimadab H, Matsubayashib N, Nishijima A, Nomura M. Accelerated deactivation of hydrotreating catalysts: comparison to long-term deactivation in a commercial plant. Catalysis Today 1998(45):319–25.

[15] Delmon B. Characterization of catalyst deactivation: Industrial and laboratory time scales. Applied Catalysis 1985(15):1–16.

[16] Novaes LdR, Pacheco ME, Salim VMM, Resende NS de. Accelerated deactivation studies of hydrotreating catalysts in pilot unit. Applied Catalysis A: General 2017;548:114–21. https://doi.org/10.1016/j.apcata.2017.06.040.

[17] Pacheco ME, Martins Salim VM, Pinto JC. Accelerated Deactivation of Hydrotreating Catalysts by Coke Deposition. Ind. Eng. Chem. Res. 2011;50(10):5975–81. https://doi.org/10.1021/ie1023595.

[18] Guichard B. Vieillissement des catalyseurs d'hydrodesulfuration: methodologie d'etude et simulation de l'evolution du site actif. Lyon: l'université Claude Bernard - Lyon 1; 2007.

[19] Mugge, B.D. and Massoth, F.E. Proc. 5th Int. Symp. Catalyst Deactivation (Surface Science and Catalysis): Mugge, B.D. and Massoth, F.E., 1991. In: C.H. Bartholomew and J.B. Amsterdam; 1991.

[20] Mugge, B.D. and Massoth, F.E. Basic studies of deactivation of hydrotreating catalysts with anthracene. Fuel Processing Technology 1991(29):19–30.

[21] Bartholdy J, ZeuthenP, Massoth F.E. Temperature-programmed oxidation studies of aged hydroprocessing catalysts. Applied Catalysis A: General 1995(129).

[22] Ahmed HS, Shaban SA, Menoufy MF, El Kady FY. Effect of catalyst deactivation on vacuum residue hydrocracking. Egyptian Journal of Petroleum 2013;22(3):367–72. https://doi.org/10.1016/j.ejpe.2013.10.006.

[23] Figoli N.S, Beitramini J.N, Querini C.A and Parera J.M. Accelerated deactivation tests in naphta reforming. Applied Catalysis 1986(26):39–45.

[24] Servia A. Using modeling to select catalyst dilution methods for mass transfer intensification in lab gas–liquid fixed-bed reactors. Oil Gas Sci. Technol. – Rev. IFP Energies nouvelles 2020;75:74. https://doi.org/10.2516/ogst/2020071.

[25] Ferrari AC, Robertson J. Interpretation of Raman spectra of disordered and amorphous carbon. Phys. Rev. B 2000;61(20):14095–107. https://doi.org/10.1103/PhysRevB.61.14095.

[26] Lauritsen JV, Bollinger MV, Lægsgaard E, Jacobsen KW, Nørskov JK, Clausen BS et al. Atomic-scale insight into structure and morphology changes of MoS2 nanoclusters in hydrotreating catalysts. Journal of Catalysis 2004;221(2):510–22. https://doi.org/10.1016/j.jcat.2003.09.015.

[27] Arancon R, Saab M, Morvan A, Bonduelle-Skrzypczak A, Taleb A-L, Gay A-S et al. Combined Experimental and Theoretical Molecular Approach of the Catalytically Active Hydrotreating MoS 2 Phases Promoted by 3d Transition Metals. J. Phys. Chem. C 2019;123(40):24659–69. https://doi.org/10.1021/acs.jpcc.9b08437.

[28] Ancheyta J, Angeles MJ, Macías MJ, Marroquín G, Morales R. Changes in Apparent Reaction Order and Activation Energy in the Hydrodesulfurization of Real Feedstocks. Energy Fuels 2002;16(1):189–93. https://doi.org/10.1021/ef0101917.

[29] Ferdous D, Dalai A. K and Adjaye J. Hydrodenitrogenation and Hydrodesulphurization of Heavy Gas Oil Using NiMo/Al2O3 Catalyst Containing Phosphorus: Experimental and Kinetic Studies. The Canadian Journal of Chemistry Engineering 2005, October, 2005:855–64.

[30] Michael J. Girgis/Bruce C. Gates. Reactivities, reaction networks, and kinetics in high-pressure catalytic hydroprocessing.

[31] Dufresne P, Bigeard P.H, Billon A.. New Developments In Hydrocracking:Low Pressure High-Conversion Hydrocracking,. Catalysis Today 1987(1):367-364.

[32] Bandyopadhyay R, Upadhyayula S. Thermodynamic analysis of diesel hydrotreating reactions. Fuel 2018;214:314–21. https://doi.org/10.1016/j.fuel.2017.10.015.

[33] Ho TC. Hydrodenitrogenation property–reactivity correlation. Applied Catalysis A: General 2010;378(1):52–8. https://doi.org/10.1016/j.apcata.2010.01.045.

[34] Speight JG. The refinery of the future. 1st ed. Amsterdam, Boston, Heidelberg: Elsevier; Gulf Professional Publishing; 2011.

[35] Gates B. C, Topsoe H. Reactivities in deep catalytic hydrodesulfurization: challenges, opportunities, and the importance of 4-methyldibenzothiophene and 4,6-dimethyldibenzothiophene. Polyhedron 1997;16(18):3213 3217.

[36] Logadóttir Á, Moses PG, Hinnemann B, Topsøe N-Y, Knudsen KG, Topsøe H et al. A density functional study of inhibition of the HDS hydrogenation pathway by pyridine, benzene, and H2S on MoS2-based catalysts. Catalysis Today 2006;111(1-2):44–51. https://doi.org/10.1016/j.cattod.2005.10.018.

[37] Brémaud M, Vivier L, Pérot G, Harlé V, Bouchy C. Hydrogenation of olefins over hydrotreating catalysts. Applied Catalysis A: General 2005;289(1):44–50. https://doi.org/10.1016/j.apcata.2005.04.014.

[38] Topsøe H. The role of Co–Mo–S type structures in hydrotreating catalysts. Applied Catalysis A: General 2007;322:3–8. https://doi.org/10.1016/j.apcata.2007.01.002.

[39] Maity S, Ancheyta J, Alonso F, Vazquez J. Study of accelerated deactivation of hydrotreating catalysts by vanadium impregnation method. Catalysis Today 2008;130(2-4):405–10. https://doi.org/10.1016/j.cattod.2007.10.009.

[40] Kanda W, Siu I, Adjaye J, Nelson AE, Gray MR. Inhibition and Deactivation of Hydrodenitrogenation (HDN) Catalysts by Narrow-Boiling Fractions of Athabasca Coker Gas Oil. Energy Fuels 2004;18(2):539–46. https://doi.org/10.1021/ef034063p.

[41] Sámano V, Rana MS, Ancheyta J. An easy approach based on textural properties to evaluate catalyst deactivation during heavy oil hydrotreating. Catalysis Communications 2020;133:105823. https://doi.org/10.1016/j.catcom.2019.105823.

[42] Callejas M.A, Martínez M.T, Blasco T, Sastre E. Coke characterisation in aged residue hydrotreating catalysts by solid-state 13C-NMR spectroscopy and temperature-programmed oxidation. Applied Catalysis A: General 2001(218):181–8.

[43] C.L. Li, O.Novaro, E. Muñoz, J.L. Boldú, X. Bokhimi, J.A. Wang, T. López,R.Gómez. Coke deactivation of Pd/H-mordenite catalysts used for C5/C6 hydroisomerization. Applied Catalysis A: General 2000(199):211–20.

[44] Anderson JR, Boudart M (eds.). Catalysis: Science and technology. Berlin, New York: Springer-Verlag; 1996.

[45] Giannetto GE, Perot GR, Guisnet MR. Hydroisomerization and hydrocracking of n-alkanes. 1. Ideal hydroisomerization PtHY catalysts. Ind. Eng. Chem. Prod. Res. Dev. 1986;25(3):481–90. https://doi.org/10.1021/i300023a021.

[46] Pirngruber GD, Maury S, Daudin A, Alspektor PY, Bouchy C, Guillon E. Balance between (De)hydrogenation and Acid Sites: Comparison between Sulfide-Based and Pt-Based Bifunctional Hydrocracking Catalysts. Ind. Eng. Chem. Res. 2020;59(28):12686–95. https://doi.org/10.1021/acs.iecr.0c01680.